A multisegment Electro-Active Polymer based milli-Continuum Soft Robots

A. Benouhiba*, K. Rabenorosoa, P. Rougeot, M. Ouisse, and N. Andreff

***Abstract*— This paper presents the design, modeling and fabrication of a millimeter-size Continuum Soft Robot (CSR). The robot consists of active flexible polymer actuator-based multisegment robot. A multiphysics model based on multilayer cantilever for large displacement is established between the input voltages to the distal tip position of a single segment robot. The extension of the model to multisegment CSR is derived. The proposed model is validated experimentally then a two-segment CSR and three-segment CSR in 3D arrangement are investigated, demonstrating the model efficiency for obtaining complex configuration. Moreover, various configurations can be explored to derive complex kinematics then increasing the robot capability.**

I. Introduction

Nature has inspired robots' design especially animals such as elephants [1] or octopus [2] for large deformation, variable stiffness, and ability to manipulate objects with various geometries, or plants for their ability to grow through environment [4], [5]. Soft robots have been investigated in the last decades, and they are subject of interest to several scientific disciplines [6], [3]. Indeed, conventional manipulator robots have rigid body and limited degrees of freedom, while soft robots have more dexterity with distributed deformation and versatility by changing shapes to access confined spaces [1], [5]. As defined in [8], "*a continuum robot is an actuatable structure whose constitutive material forms curves with continuous tangent vectors*". Various robots considered as continuum, once they have been developed, they can be classified according to the structure – single backbone [8] or multibackbone [12], [13], and the actuation principle – extrisinc or intrinsic one. Continuum soft robot (CSR) is a class that combine soft body and continuum structures as shown in Fig. 1. It includes some developed robots as reviewed in [3], [8], [14]. CSRs present a design challenge considering their actuation and sensing mechanisms, often are highly integrated with the robot body. Recent advances in additive manufacturing and 3D printing have allowed fabrication of proof of concept at conventional scale. Reaching smaller scales (from centimeter to micrometer-scale), CSR remains an open challenge by considering the miniaturization difficulty of fabrication process [14]. Electrically responsive soft actuators are investigated and Electro-Active Polymers (EAP) constitute a solution with great potential [15]. The recent developments of Conducting Polymer (CP), which are compatible to small scales [16], [17], have enabled to achieve complex and innovative soft robots [18], [19]. Some recent works can be classified as milli-CSR : Chikhaoui et al. for a telescopic soft robot based on CP actuator [9], Wang et al. for a serial multisegment flexible soft robots actuated by Ionic Polymer–Metal Composites (IMPC) [7] or Ikeuchi and Ikuta [21] for a pneumatically actuated two-segment catheter, or Moghadam et al. for a continuum soft parallel robot [11].

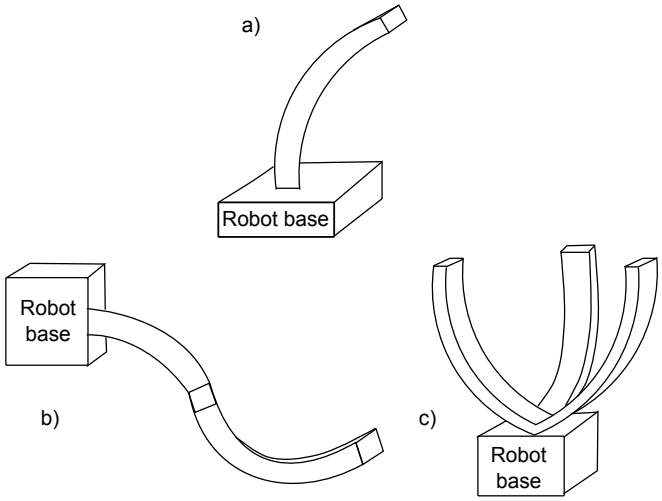

Fig. 1. Concepts of CSR with a) single segment, b) two-segment series, and c) three-segment in parallel.

In this paper, we propose to investigate a multisegment EAP based millimeter-size CSR. The main objective of this work is to present a modeling, fabrication and experimental validation of compact and energy efficient multisegment CSR with large deformation capability by using PolyPyrrole (PPy) based conducting polymers. In addition, proof-of-concept of multisegment CSR is provided. CP is an EAP with numerous advantages as low actuation voltage (usually less than 1V), large deformation (up to 30%), low fabrication cost, and biocompatible. First, a modeling of large deformation CP is proposed, derived from compact multilayer model which enables to predict large deformation in complement to the model limitation discussed in [20]. It is described in Section II and completed with its extension to serial multisegment and 3D multisegment. Section III details fabrication and experimental validation. Finally, Section IV concludes the paper.

* Corresponding author

All authors are with FEMTO-ST Institute, Univ. Bourgogne Franche-Comté/CNRS, 25000 Besançon, France. name.surname@femto-st.fr

TABLE I

LIST OF VARIABLES.

Variables	Definition	Value	Unit
E_1/E_3	Young's modulus of the first/third layers of PPy	80×10^6	Pa
E_2	Young's modulus of the second layer of PVDF	440×10^6	Pa
t_1/t_3	Thicknesses of the first/third layers of PPy	7.5×10^{-6}	m
t_2	Thickness of the second layer of PVDF	55×10^{-6}	m
b	Width of the multilayer cantilever	1×10^{-3}	m
L	Length of the multilayer cantilever	27×10^{-3}	m
α	Corrective factor	1.226×10^{-1}	$(F/m^2)/(C/m^3)$
C	Volumetric capacitance	4×10^8	F/m^3
DV	Input voltage	$0.1<DV<0.7$	V

II. Modeling EAP-based multisegment milli-CSR

This section introduces a static large-deflection model of a multilayer cantilever. First, there is few assumptions to be considered :

— i represents the index for a layer.
— the material of each layer remains linearly elastic.
— two consecutive layers are perfectly bonded.
— the radius of the curvature ρ of the multimorph cantilever cause by the combined effect of all stresses is much bigger than its thickness.

The model is derived from the non-linear Euler-Bernoulli beam equation. For x, a position between 0 and L the length of the multilayer cantilever (as shown in Fig. 2), it writes :

$$\frac{1}{\rho}=\frac{M_{eq}}{(EI_{eq})}=\frac{\sum_{i=1}^{n}M_i}{\sum_{i=1}^{n}E_iI_i}=\frac{d\theta}{ds}=\frac{\frac{d^2y}{dx^2}}{(1+(\frac{dy}{dx})^2)^{\frac{3}{2}}} \quad (1)$$

where M_i is the individual bending moment and E_iI_i is the flexural rigidity.

An induced longitudinal strain at any level of the multilayer cantilever, causes a bending moment, which can be considered as constant across $\overline{AC}$ (as shown in Fig. 2), since the cross-section of the cantilever is uniform along its length. An analytical solution of eq. 1 for a linear elastic material multilayer cantilever, was proposed by Kim et al [22]. It was given by direct integration and application of the boundary conditions, $y'(0)=0$ and $y(0)=0$, hence, the shape of the whole beam (solution of eq. (1)) is determined as follows :

$$\frac{x}{\rho}=\frac{\frac{dy}{dx}}{(1+(\frac{dy}{dx})^2)^{\frac{1}{2}}} \quad (2)$$

$$y=\rho\left(1-\sqrt{(1-\left(\frac{x}{\rho}\right)^2)}\right) \quad (3)$$

and since the length of the unbent multilayer cantilever $\overline{AB}=L$, is the same as the one of the bent cantilever $\overline{AC}$, the horizontal deflection can be determined with the arc length $ds=\sqrt{1+(dy/dx)^2}$, in addition :

$$L=\int_0^{L-\delta x}\sqrt{1+\left(\frac{dy}{dx}\right)^2}\,dx \quad (4)$$

And by using the trigonometric substitution, $x=\rho.sin\theta$, the tip deflection of the multilayer cantilever can be obtained as such :

$$\delta x=L-\rho.sin\left(\frac{L}{\rho}\right) \quad (5)$$

$$\delta y=\rho\left(1-cos\left(\frac{L}{\rho}\right)\right) \quad (6)$$

Moreover, the eq. (5) and eq. (6) assume that the multilayer cantilever maintains its linear elastic properties during large deformation. This is true for typical thin Micro Electro-Mechanical System (MEMS), which is indeed the case here.

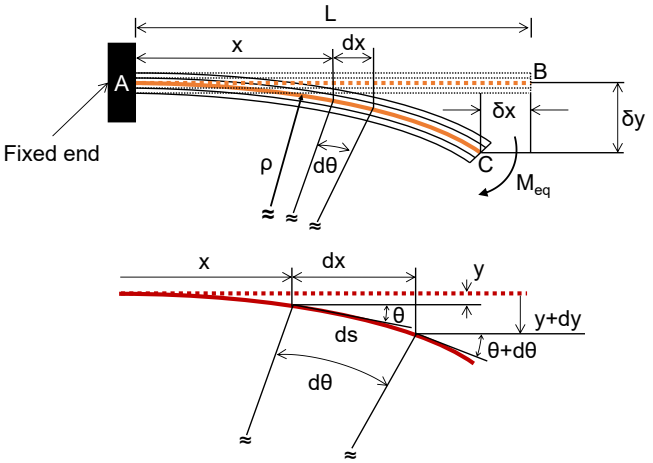

Fig. 2. Description of large deflection of multilayer cantilever adapted from [22].

A. Single segment model

This section models the behavior of trilayer electro-active actuator, composed of two PPy active layers, and a porous PolyVinylidene DiFluoride (PVDF) passive layer. The variable list is given in Tab. I. Furthermore, the radius of the curvature ρ is derived according Kim et al [22] :

$$\rho=\frac{2RA^{-1}S}{2+RA^{-1}B} \quad (7)$$

where :

$$R=\frac{-1}{E_1I_1+E_2I_2+E_3I_3}\left[\left(\frac{t_1}{2}\right)\left(t_1+\frac{t_2}{2}\right)\left(t_1+t_2\frac{t_3}{2}\right)\right] \quad (8)$$

$$A = \begin{bmatrix} \frac{1}{E_1 I_1} & \frac{-1}{E_2 I_2} & 0 \\ 0 & \frac{1}{E_2 I_2} & \frac{-1}{E_3 I_3} \\ 1 & 1 & 1 \end{bmatrix} \tag{9}$$

$$B = \begin{bmatrix} t_1 + t_2 \\ t_2 + t_3 \\ 0 \end{bmatrix} \tag{10}$$

and

$$S = \begin{bmatrix} \varepsilon_2 - \varepsilon_1 \\ \varepsilon_3 - \varepsilon_2 \\ 0 \end{bmatrix} \tag{11}$$

In eq. (11) the strain ε_2 of the second layer is null, considering the fact that it is a passive layer. However, the strain for the first/third layers are : $\varepsilon_1 = 2\alpha \frac{C.DV_1}{t_1 b L E_1}$ and $\varepsilon_3 = 2\alpha \frac{C.DV_3}{t_3 b L E_3}$, and since $DV_1 = -DV_3$, which is essential to activate the trilayer microactuator, thus, the eq. (11) can be written as follows :

$$S = \begin{bmatrix} 2\alpha \frac{C.DV}{t_1 b L E_1} \\ 2\alpha \frac{C.DV}{t_3 b L E_3} \\ 0 \end{bmatrix} \tag{12}$$

Furthermore, by using eq. (8) (9) (10) (12) and (7), the radius of the curvature of the trilayer microactuator, ρ is equal to :

$$\frac{(t_1+t_2)\left(\frac{E_1E_3I_1I_3\psi_2}{\psi_1} - \frac{\psi_3}{2\psi_1} + \frac{E_1E_2I_1I_2\left(t_1+\frac{t_2}{2}\right)}{\psi_1}\right) - (t_2+t_3)\left(\frac{\psi_5}{2\psi_1} - \frac{E_3I_3\psi_4\psi_2}{\psi_1} + \frac{E_2E_3I_2I_3\left(t_1+\frac{t_2}{2}\right)}{\psi_1}\right) + 2}{\frac{C.DV\alpha\left(\frac{E_1E_3I_1I_3\psi_2{}^2}{\psi_1} - \frac{\psi_3}{2\psi_1} + \frac{E_1E_2I_1I_2\left(t_1+\frac{t_2}{2}\right)^2}{\psi_1}\right)}{E_1 L b t_1} - \frac{C.DV\alpha\left(\frac{\psi_5}{2\psi_1} - \frac{E_3I_3\psi_4\psi_2{}^2}{\psi_1} + \frac{E_2E_3I_2I_3\left(t_1+\frac{t_2}{2}\right)^2}{\psi_1}\right)^2}{E_3 L b t_3}} \tag{13}$$

Where :
$\psi_1 = (E_1I_1 + E_2I_2 + E_3I_3)^2$
$\psi_2 = t_1 + t_2 + \frac{t_3}{2}$
$\psi_3 = E_1I_1t_1(E_2I_2 + E_3I_3)$
$\psi_4 = E_1I_1 + E_2I_2$
$\psi_5 = E_1E_3I_1I_3t_1$

Then, eq. (13) was used to calculate the tip deflection of the trilayer microactuator, along the x and y axis, as shown in the expressions (5) (6). However, for the sake of convenience, the fully developed expressions of the tip deflection will not be expressed here.

B. multisegment model

This subsection aims to model the behavior of the multisegment EAP based CSR, however, since the basic unit for the latter is the trilayer microactuator, this model will be an extension of the model discussed above. Each segment is modeled separately, then, by the continuity principle, all of the segments are connected once again, after the deformation, hence, modeling the behavior of a complex multisegment CSR, can be possible. Among the various types of the multisegment CSR, we choose to present the following categories :

1) Two-segment CSR: The two-segment CSR is a serial type soft robot, with two segments attached serially. It can have more than two serially linked segments, however, for the sake of simplicity this paper will only discusses the two-segment one. Furthermore, when it comes to the model, and as stated above, each segment will be modeled separately, then, the base of the second segment will be attached to the end of the first one, using a small transition part (a few mm long). The latter is straight part tangent to the first segment at its tip, as shown in Fig. 3. Its main role is to insure that the second segment is correctly attached and that it has a suitable orientation.

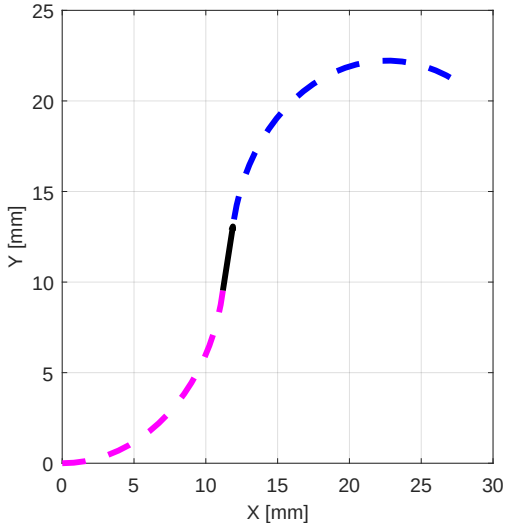

Fig. 3. The model for a 1 *mm* wide two-segment CSR, with a first segment of 16 *mm*, a transition part of 5 *mm* and a second segment of 20 *mm*, under an applied voltage of 0.5 *V*.

2) Four-segment CSR: The second type of the multisegment CSR has four segments, where all of then have the same base. Nonetheless, each segment is rotated with a certain angle from its neighbor, in this case 90°, as shown in Fig. 4.

3) Eight-segment CSR: The multisegment CSR in this case is a combination of the two above, meaning, four parts with same base, oriented at 90° from one to another, and each part is composed of a two-segment CSR. The configuration of this CSR obtained by the proposed model is shown in Fig. 5.

III. Experimental validation

The main objective of the section is to discuss the fabrication of different types of the CSR, starting by the trilayer microactuator. Next, the characterizations of the deformation curvature for the single and two-segment CSR are presented, and then comparing the results to the model discussed above, for validation. Finally a proof of concept of a more complex multisegment CSR is presented.

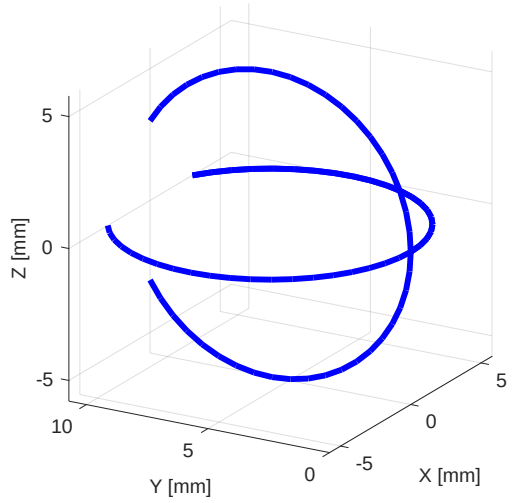

Fig. 4. The model of a four-segment CSR, where each segment is 15 *mm* long and 1 *mm* wide, under an applied voltage of 0.7 *V*.

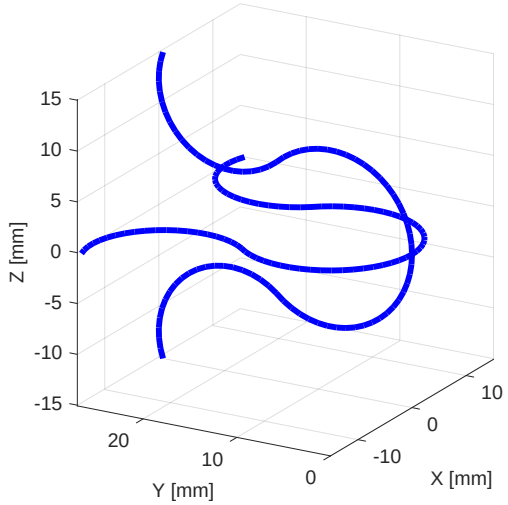

Fig. 5. The model of a eight-segment CSR, where each segment is 15 *mm* long and 1 *mm* wide, under an applied voltage of 0.7 *V*.

A. *Fabrication*

The fabrication of the trilayer microactuator was done using an electropolymerization process. First, a PVDF membrane Immobilion P from Millipore (product specifications : pore size 0.45 μm, porosity 70%), was previously covered by a layer of chromium/platinum with a thickness of $10/50\,nm$ on both sides, using a cathodic sputtering process. This step is crucial, since the conductive properties of PVDF membrane, are necessary for the electropolymerization process. However, the added layers can also generate unwanted residual stresses, that can have a very negative effect on the final microactuator. Then, the PVDF membrane was mounted on a standard three-electrodes system (as shown in Fig. 6), as a working electrode, for the electropolymerization process.

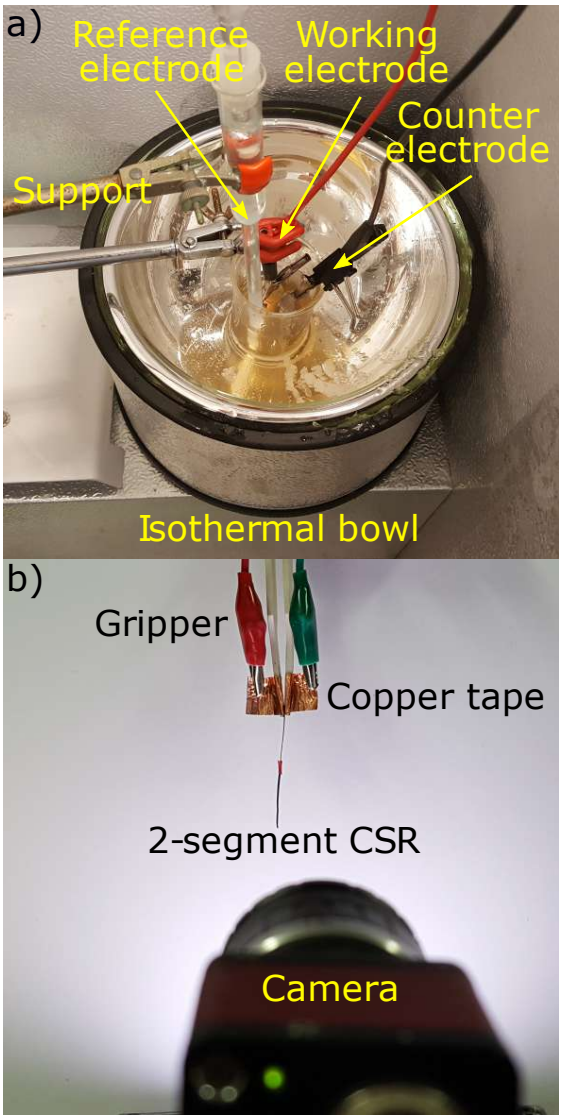

Fig. 6. a) Electropolymerization system with three electrodes put inside a freezer during PPy growing, and b) the experimental setup for characterization of the proposed CSRs.

The three-electrode system was also composed of Ag/AgCl reference electrode and a platinum grid counter electrode. The former system was linked to a potentiostat, OrigaFlex-OGF500 (from OrigaLys ElectroChem SAS), which was controlled by OrigaMaster5 [1] software. The process is similar to the one proposed in the work of Cot et al [20] but the electropolymerization setup is based on a more accurate potentiostat. After the electropolymerization process, the final product was cleaned using acetone, then cut by a very sharp scalpel to a 1 *mm* wide strips, to be used in the experimental setup afterwards.

1. `http://www.origalys.com/origasoft-logiciel-pc-\origamaster-c2x19668303`

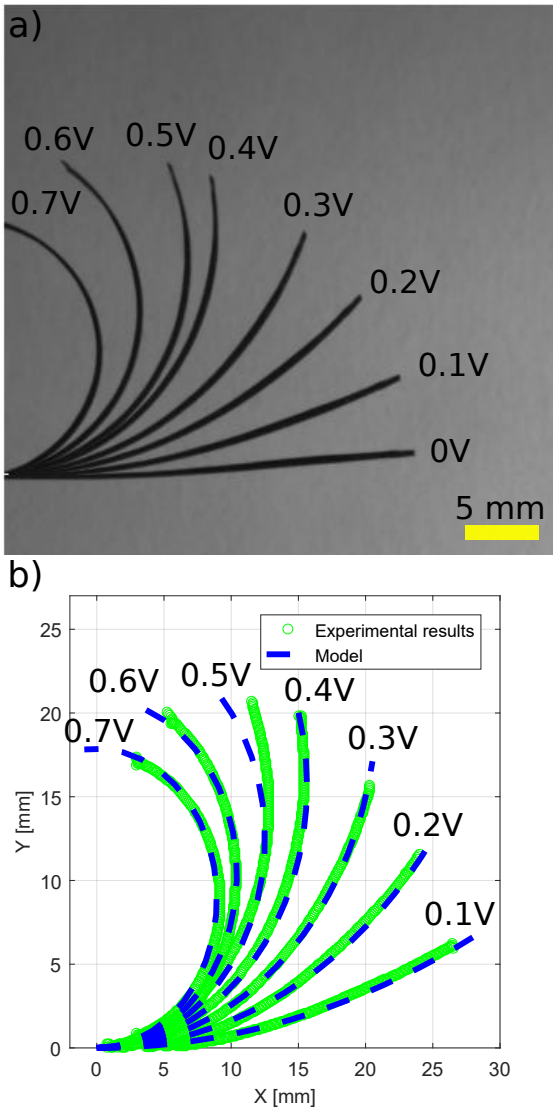

Fig. 7. Single segment CSR experimental validation : a) the responses for an applied voltage varying from 0.1 to 0.7 V obtained through The overlay of images, and b) comparison of the experimental results to the model.

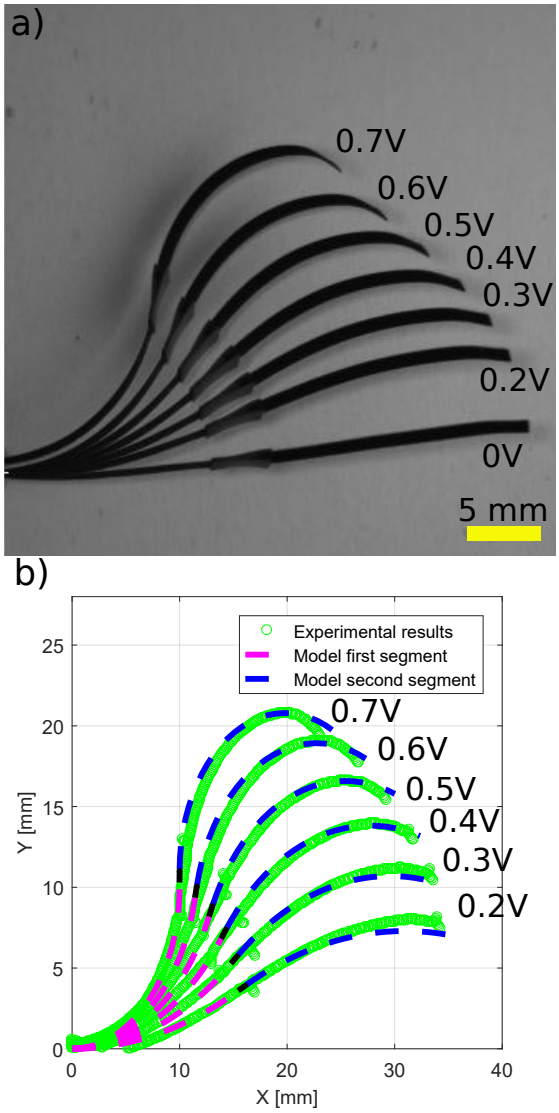

Fig. 8. Two-segment CSR experimental validation : a) the responses for an applied voltage varying from 0.1 to 0.7 V obtained through The overlay of images, and b) comparison of the experimental results to the model (dashed line, red for the first segment and blue for the second segment).

B. Experimental setup

In order to characterize the designed CSR, a test bench is developed based on MATLAB Simulink software using Visual Servoing Platform (ViSP) with a dedicated blockset cvlink [2]. The CSR is held at its base by a small gripper made conductive with copper tape (Fig. 6). Voltage is provided via a National Instruments multifunction data acquisition module (USB-6211), which can manage a voltage between $\pm$ 10 V with a resolution of 3.5 mV. The camera (IEE 1394 Guppy Firewire) is positioned in front of the actuation platform (as shown in Fig. 6) in order to visualize the side of the actuator in its thickness. The dimensions of the considered two-segment CSR is about 16×1 mm^2 for the first segment and 20×1 mm^2 for the second segment.

2. https://sourcesup.renater.fr/cvlink/

C. Model validation

This subsection contains the experimental validation of the model for the PPy microactuator, and in order to do so, a series of experimental tests was conducted. The process starts by cutting a 27 mm long and 1 mm wide trilayer PPy microactuator, and hang it from one end in front of the camera, as mentioned above. Then, for each test a voltage is applied, during 25 s, while the camera is recording. The 25 s duration is required to ensure that the PPy microactuator has reached the steady state and its maximum deformation under the applied voltage. The latter varies from 0.1 to 0.7 V (higher voltages can damage the PPy microactuator). Afterwards the PPy microactuator gets a 30 s rest time, in order to go back to its former state (zero deformation). In the next step, the videos were decomposed into frames, and then,

the frames corresponding to the maximum deformation were used to determine the curvature of the PPy microactuator for each applied voltage. The information was initially given in pixels, therefore, it was converted, to mm and then, compared to the results of the model, as shown in Fig. 7. The model is compared to experimental results and the measured error is presented in Tab. II. The mean error is less than 1 *mm* which corresponds to 3.7% of the segment length, which is considered to be satisfactory.

TABLE II
THE ERROR OF THE SINGLE-SEGMENT MODEL.

RMS (μm)	STD (μm)	MAX (μm)	MIN (μm)
840	555	1677	2

D. Two-segment CSR characterization

In order to characterize the two-segment CSR, a strip of trilayer PPy actuator was cut to a width of 2 *mm*. Then, in approximately its middle, its width was narrowed down, by cutting of small rectangular pieces of it, from each side. As a result, the concerned zone became very flexible, therefore twisting the actuator by 180° at this area was feasible. The actuator was held in the twisted state by a tiny strip of duct tape. The final product was a two-segment CSR, 16 *mm* long first segment, 1 *mm* rigid link, and a 20 *mm* long second segment. The rigid link is very important for two-segment CSR because it ensures the electric connection to the second segment, that way the latter can achieve high deformations as well as the first segment. As for the characterization of the two-segment CSR, the latter was mounted on the experimental setup, and a series of experimental tests similar to those discussed above were conducted. Finally, the deformation of the two-segment CSR for the different applied voltages was compared to the model, as shown in Fig. 8.

TABLE III
THE ERROR OF THE TWO-SEGMENT MODEL.

RMS (μm)	STD (μm)	MAX (μm)	MIN (μm)
356	209	864	21

The proposed two-segment model is able to simulate the large deformation generated by the two-segment CSR. The RMS error for the different actuation voltages is about 356 μm, and the STD error is 209 μm (as shown in Tab. III). One can conclude that the model works well then it can be used for later development.

E. Proof of concept of more complex CSR

In this subsection, a three-segment CSR was fabricated by cutting three strips of the trilayer microactuator, each one is 8 *mm* long and 1 *mm* wide. The strips then were placed in top of 3D printed model of the three-segment CSR, in order to insure that all of the three segments are oriented at 120° form one another. Next, using a small piece of an adhesive copper tape, the three segment were fixed at their proximal ends. Finally, the excess copper tape was carefully cut. For this demonstration, the three-segment CSR was side viewed

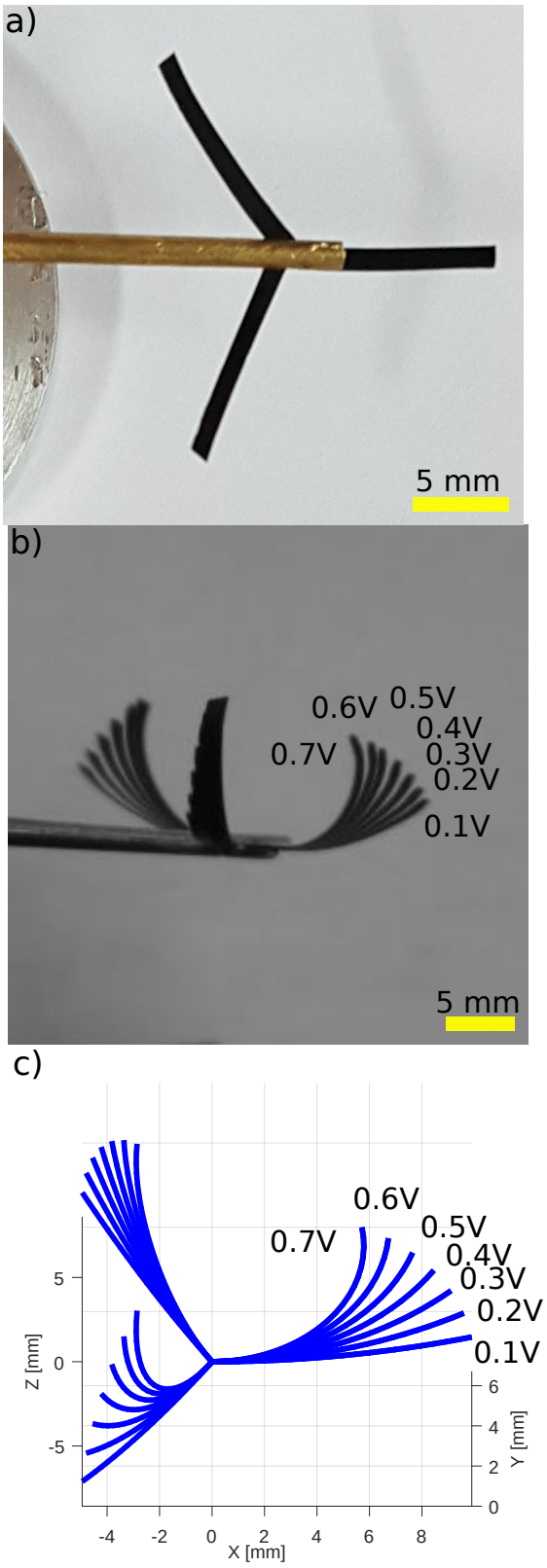

Fig. 9. a) Top view of the three segment CSR, b) the overlay of images for an applied voltage varying from 0.1 to 0.7 *V*, and c) the corresponding model results.

by a camera and held by two long copper parts. One was used to press on the copper tape, and the second to press against all of the three-segment at the same time, from the other side (as shown in Fig. 9).

It was demonstrated that the fabricated three-segment CSR is functioning and consequently the fabrication process is validated. In addition, this result opens the possibility to design multi-arm collaborative robots at small scales.

IV. Conclusions

In this paper, a multisegment electro-active polymer based CSR is introduced. The fabrication process of such CSR was discussed, as well. A large deformation analytical model of the single and two-segment CSR was also introduced and experimentally validated with a good accuracy. Moreover,more complex configurations of the multisegment CSR was investigated with details on the fabrication process and its functioning was demonstrated.

The development of such CSR can be very beneficial for a lot of applications, especially, applications where navigating through constrained environment, is a major concern, such as, biomedical applications and manipulation at small scales. The multisegment CSR can navigate in narrow spaces either by itself, or by using its surrounding as a support, when the deformation needed is very important even for it. Furthermore, inserting more than one multisegment CRS should be possible, so collaboration between the robots can be envisioned.

The next step will be the investigation of higher number of multisegment CSR, which constitutes a multi-arm collaborative robot. It will enlarge the workspace and improve dexterity of a complex CSR. In addition, controlling each CSR separately or together for achieving a task will be an interesting challenge. The complexity of the shape can be increased by using laser micromachining, this approach is under development.

ACKNOWLEDGMENT

This work has been supported by EUR EIPHI (Contract No. ANR-17-EURE-0002), CoErCIVe Bourgogne Franche-Comté regional project, and μRoCS project (contract ANR-17-CE19-0005-04).

References

[1] Trivedi, D., Rahn, C. D., Kier, W. M., & Walker, I. D.,"Soft robotics : Biological inspiration, state of the art, and future research". *Applied bionics and biomechanics*, 5(3), 99-117, 2008.

[2] Laschi, C., Cianchetti, M., Mazzolai, B., Margheri, L., Follador, M., & Dario, P., "Soft robot arm inspired by the octopus". *Advanced Robotics*, 26(7), 709-727, 2012.

[3] Laschi, C., Mazzolai, B., & Cianchetti, M. "Soft robotics : Technologies and systems pushing the boundaries of robot abilities". *Science Robotics*, 1(1), 2016.

[4] Mazzolai, B., "Plant-inspired growing robots". In *Soft Robotics : Trends, Applications and Challenges*. Springer, Cham, pp. 57-63, 2017.

[5] Hawkes, E.W., Blumenschein, L.H., Greer, J.D. and Okamura, A.M., "A soft robot that navigates its environment through growth". *Science Robotics*, 2(8), p.eaan3028, 2017.

[6] Rus, D., & Tolley, M. T., "Design, fabrication and control of soft robots". *Nature*, 521(7553), 467, 2015.

[7] Wang, H., Chen, J., Lau, H. Y., & Ren, H., "Motion planning based on learning from demonstration for multiple-segment flexible soft robots actuated by electroactive polymers". *IEEE Robotics and Automation Letters*, 1(1), 391-398, 2016.

[8] Burgner-Kahrs, J., Rucker, D.C., & Choset, H., "Continuum robots for medical applications : A survey". *IEEE Transactions on Robotics*, 31(6), pp.1261-1280, 2015.

[9] Chikhaoui, M. T., Cot, A., Rabenorosoa, K., Rougeot, P., & Andreff, N., "Design and closed-loop control of a trilayer Polypyrrole based telescopic soft robot". In *IEEE/RSJ International Conference on Intelligent Robots and Systems*, pp. 1145-1150, 2016.

[10] Chikhaoui, M. T., Rabenorosoa, K., & Andreff, N. (2018). "Inverse Kinematics Analysis of a P2CuP2Cu Concentric Tube Robot with Embedded Micro-actuation for 3T-1R Contactless Tasks". In *Advances in Robot Kinematics*, Springer, Cham. , pp. 51-59, 2016.

[11] Moghadam, A. A. A., Kouzani, A., Torabi, K., Kaynak, A., & Shahinpoor, M., "Development of a novel soft parallel robot equipped with polymeric artificial muscles". *Smart Materials and Structures*, 24(3), 035017, 2015.

[12] Xu, K., & Simaan, N., "Intrinsic wrench estimation and its performance index for multisegment continuum robots". *IEEE Trans. Robot.*, pp. 555–561, Jun. 2010.

[13] Kang, B., Kojcev, R. & Sinibaldi, E., "The first interlaced continuum robot, devised to intrinsically follow the leader". *PloS one*, 11(2), p.e0150278, 2016.

[14] Hines, L., Petersen, K., Lum, G.Z. & Sitti, M., "Soft Actuators for Small–Scale Robotics". *Advanced Materials*, vol.29, num. 13, 2017.

[15] Bar-Cohen, Y. "Electroactive polymers as artificial muscles-reality and challenges". In *19th AIAA Applied Aerodynamics Conference*, p. 1492, 2001.

[16] Jager, E. WH, E. Smela, & O. Inganäs. "Microfabricating conjugated polymer actuators". *Science*, pp. 1540-1545, 2000.

[17] Nguyen, N. T., Plesse, C., Vidal, F., Soyer, C., Grondel, S., Madden, J. D., & Cattan, E., "Microfabricated PEDOT trilayer actuators : synthesis, characterization, and modeling". In *Electroactive Polymer Actuators and Devices (EAPAD)*. International Society for Optics and Photonics, vol. 10163, p. 101631K, 2017.

[18] Mutlu, R., Alici, G. & Li, W., "A soft mechatronic microstage mechanism based on electroactive polymer actuators". *IEEE/ASME Transactions on Mechatronics*, 21(3), pp.1467-1478, 2016.

[19] Mutlu, R., Alici, G. & Li, W., "Three-dimensional kinematic modeling of helix-forming lamina-emergent soft smart actuators based on electroactive polymers". *IEEE Transactions on Systems, Man, and Cybernetics : Systems*, 47(9), pp.2562-2573, 2017.

[20] Cot, A., Chikhaoui, M. T., Rabenorosoa, K., Rougeot, P., & Andreff, N., "Synthesis, encapsulation, and performance analysis of large deformation trilayer polypyrrole actuator". In *IEEE International Conference on Advanced Intelligent Mechatronics*, pp. 436-441, 2016.

[21] Ikeuchi, M., & Ikuta, K., "Membrane micro emboss following excimer laser ablation (MeME-X) process for pressure-driven micro active catheter". in *IEEE 21st International Conference on. Micro Electro Mechanical Systems (MEMS)*, 2008.

[22] Kim, J. I., "Compact multiphysics models for large-displacement multilayer cantilevers in RF MEMS circuits, antennas and sensors". *Doctoral dissertation, Purdue University*, 2008.